# **Enhancing the Mechanical Performance of Carbon Fiber Reinforced Polymer Using Carbonized Coconut Shell Particles**

Foster Feni<sup>1</sup>, Maryam Jahan<sup>2</sup>, Fareed Dawan<sup>1</sup>, Samuel Ibekwe<sup>1</sup>, Guoqiang Li<sup>1,3</sup>, Patrick Mensah<sup>1</sup>

<sup>1</sup>Mechanical Engineering Department, Southern University and A&M College, Baton Rouge, LA 70813, USA

<sup>2</sup>Chemistry Department, Southern University and A&M College, Baton Rouge, LA 70813, USA

<sup>3</sup>Department of Mechanical & Industrial Engineering, Louisiana State University, Baton Rouge, LA 70803

## **Abstract**

Inorganic fillers have been used to improve the out-of-plane mechanical properties of carbon fiber reinforced polymer (CFRP) composite laminates for decades. Nonetheless, its associated high cost and environmental unfriendliness is a concern. Biomaterials are currently being explored as fillers in polymeric materials due to their low cost, wide availability, and biodegradability. However, the use of coconut shell based biofillers together with carbon fibers in epoxy matrix has not been investigated. This research seeks to improve the out-of-plane mechanical properties of CFRP with low fiber volume fraction using carbonized coconut shell particles (CCSP). Five hybrid epoxy biocomposites with varying concentrations of CCSP were used to impregnate four plies of woven carbon fabric, making up a fiber volume fraction of 29%. The tensile, flexural, and impact behavior of the laminated biocomposites were investigated. The mechanical properties of the biocomposite laminates were enhanced compared to a reference CFRP without CCSP. This work provides a cheaper and greener alternative to inorganic CFRP hybrid composite for potential use in automotive and aerospace industries.

Keywords: Biocomposite, impact test, out-of-plane, coconut shell, laminated composite

## 1. Introduction

Carbon Fiber Reinforced Polymer (CFRP) composite laminates are increasingly being utilized in structural applications because of their superior in-plane characteristics, including high specific strength and stiffness, low thermal expansion, resistance to corrosion and ease of processing [1,2]. Nonetheless, they possess poor and unpredictable out-of-plane properties that translates into weak cracking resistance and delamination, thereby making them susceptible to failure in the event under out-of-plane or multi-axial loading, particularly, impact or blast [3,4]. To harness the full potential of Fiber Reinforced Composites in the automobile, renewable energy generation, structural and aerospace industry, it is necessary to improve their out-of-plane properties to avert catastrophic failure. Past studies which characterize the interphase viscoelastic properties in a sandwich glass composite [5] and the effect of resin uptake on the flexural properties of compression molded sandwich composites [6], have demonstrated the importance of enhanced off-axis properties. These research have shown that the out-of-plane properties are usually matrix dominant; low interlaminar shear strength, and low bonding strength at the fiber-matrix interface affect energy dissipation, and could lead to delamination, and subsequent failure from crack propagation [4,5]. In essence, the matrix properties play a crucial role in the failure mechanism of Fiber Reinforced Polymer (FRP). Epoxy resin is the most extensively utilized polymer matrix in the fabrication of composite for structural and automobile applications owing to its ease of processability, high strength, and chemical resistance [8]. Despite its numerous advantages, it has low toughness and is susceptible to mechanical failure when subjected to substantial amount of mechanical load. The brittleness of epoxy results from limited chain mobility due to its highly crosslinked structure [9].

To overcome the shortcoming of FRPs, researchers have used inorganic and synthetic particulates of alumina [8-10], titanium oxide [11,12], silica [11,13,14] and various forms of carbon nanotube (CNT) [3, 15-18] as toughening materials to enhance the mechanical properties of FRPs. For instance, a study has been reported in literature on the potential enhancement of interfacial compressive strengths of CFRP composites using scrolling carbon nanotube (CNT) sheets around individual carbon fibers [21]. Fiber push-out and fiber push-in nanoindentation experiments were carried out; results showed improved interfacial shear strength of CNT/CFRP compared to CFRP that bodes well for structural applications. Addition of particulates to polymer matrices enhances the performance of composite in multiscale by mechanism of crack-pinning and crack path deflection [3,4,7]. However, the cost involved in processing these fillers is skyrocketing, their processing is complicated with lots of difficulties, and they are abrasive to tools.

The main aim of this study is to enhance the out-of-plane mechanical behavior of CFRP by fabricating a hybrid biocomposite using biofiller as an alternative to synthetic and inorganic particulates. Organic materials have shown great promise of being used as fillers in polymers for biocomposites. They are highly desired due to their low cost, good mechanical properties, low densities, high toughness, biodegradability and good thermal properties [22]. Many studies have been conducted for the possibility of using organic waste of groundnut shells, coconut shells, jute fibers, sisal fibers, bamboo and rice husk as reinforcement either in the form of fiber or particle for biocomposites [25-31].

Coconut shells have gained much interest as biofillers in polymers, for their availability, and inherent mechanical properties [19,26]. The tensile property and hardness of epoxy resin has been improved with the addition of 50% and 5% coconut shell powder and tamarind shell powder respectively [30]. Agunsoye investigated epoxy reinforced with coconut shell particle for car bumper applications [31]. The biocomposite showed 10% increase in impact energy in comparison to bumpers from two different car models. Additionally, Uchechi investigated the effect of carbonized coconut shell particles on polypropylene [32]. The resulted biocomposite showed an increase in hardness, tensile and flexural properties with an increase in filler concentration and decrease in particle size.

Coconut shell particles have been used as fillers to toughen and strengthen many polymer matrices. However, to the best of our knowledge, no work has been done in employing carbonized coconut shell particle to form a hybrid biocomposite with CFRP. This study endeavors to improve the mechanical performance of CFRP using carbonized coconut shell particle (CCSP) to form a hybrid biocomposite. In this investigation, coconut shells were carbonized in an electrothermal furnace at 400°C to form activated carbon which was used to fabricate a hybrid biocomposite with four plies of carbon fiber and epoxy matrix. Five hybrid biocomposites were fabricated with different matrices containing 1, 2, 3, 4, and 5% weight concentration of CCSP in epoxy, and compared with a reference CFRP based on bare epoxy and 29% volume fraction of woven carbon fabric. The tensile, flexural, and impact properties of the composites were investigated. The fractured surface of reference and hybrid composites were characterized by Scanning Electron Microscopy (SEM).

#### 2. Materials and Methods

#### 2.1. Materials

Coconut shells were obtained from a local shop. Aeromarine-based cycloaliphatic epoxy resin #300 and hardener #21 were used as reagents supplied by Aero Marine Products Inc., USA. This type of epoxy was chosen for its low viscosity, excellent chemical resistance, and good bonding behavior with carbon fibers. 3K plain woven Carbon fabric from Fiber Glast Development Corp. (Ohio, USA) with an aerial weight of 190 g/m² was selected as base reinforcement, for its lightweight and high strength.

## 2.2. Preparation of carbonized coconut shell particles

The step-by-step process of the preparation of CCSP is shown in Supporting Information *Figure S1*. Coconut shells (CS) obtained were crushed to small sizes to allow for easy handling. The shells were washed in 0.5 HNO<sub>3</sub> acid at a temperature of 60°C/70°C for 8 hours as shown in the second step of *Figure S1*. This was necessary to clean CS of any fruit remains and oily substance. The cleaned CS was rinsed and filtered with distilled water until the pH of the water filtered was close to 7, to ensure complete wash of acid. It was dried in air for 48 hours and pulverized into powder. The powdered CS was then heated in an electrothermal furnace for 2 hours at 400°C. The resulting product was ball milled into fine powder resulting in an average particle size of 300nm and used in the preparation of the hybrid composite. The precursor before carbonization (raw coconut particles) and after carbonization (CCSP) were analyzed using Scanning Electron Microscopy (SEM), Fourier Transform Infrared (FTIR) and X-ray Diffraction (XRD).

# 2.3 Fabrication of hybrid composite

The composites were fabricated utilizing the hand lay-up method with a 200mm X 200mm detachable closed mold. In the Supporting Information, *Figure S2* shows a step-by-step process in the fabrication of hybrid biocomposites. Five hybrid composites with different compositions of CCSP: 1%, 2%, 3%, 4% and 5% were fabricated. These compositions are weight fractions of the epoxy used. These proportions of CCSP were weighed and added to 200g of epoxy and mixed thoroughly using a mechanical stirrer for 5 hours at room temperature to ensure uniformity. 100g of hardener was then added, and hand stirred for an additional 15 minutes. Four sheets of woven carbon fabrics, each cut into the size of the mold, were then impregnated with the mixture and laid in longitudinal direction for each ply using the hand lay-up method. The mold was covered, placed under a compressive pressure of 700N/cm², and the composite was cured for 48 hours at room temperature. The reference sample named 'bare' was also fabricated using the same procedure. However, no CCSP was added to the resin. The matrix used was based on bare epoxy and hardener, together with four plies of plain-woven carbon fabric. For low velocity impact test, eight sheets of woven carbon fiber were used (instead of four) in each composite system to achieve a thickness of 4.10mm.

#### 2.4 Mechanical characterization

The final rectangular composite laminate of dimension, 228.6mm X 228.6mm and a thickness of 2mm was cut into required sizes for mechanical testing. Rectangular coupons of 200mm X 25.6mm were cut from the cured composites for the purpose of tensile testing according to ASTM D 3039 [33], at a displacement rate of 2mm/min. Rectangular samples are usually preferred over dog-bone in characterizing tensile properties of composites as the dog-bone usually split at the regions where width changes [34]. Grip tabs of glass fiber/epoxy laminates with

dimension 25.4mm X 38.1mm was bonded to the ends of the test specimen to minimize large stress concentrations at these regions, resulting in a gauge length of 125mm.

Flexural testing was performed to investigate the resistance of composites to deflection. A three-point bending fixture of the MTS universal testing machine was used at a loading rate of 2mm/min. Each specimen has a width of 12.5mm and a thickness of 2mm. A span length of 35mm was used.

An Instron Dynatup 8250 impact tester was used to perform a low-velocity impact test on the reference CFRP and hybrid biocomposites. The dimension of each sample is 102mm X 25.4mm with a thickness of 4.10mm. The impact hammer used in striking the specimen weighed 11.22kg and fell from a height of 205mm to achieve a velocity of 2m/s. An instrumental load cell attached to the instrument was used to collect data of load and energy absorbed.

## 2.5 Powder characterization

XRD analysis was performed on both precursor (raw coconut) and char (CCSP) to identify the phase formed. XRD measurement was performed from an angle of 5° to 80° at a step rate of 0.2° using MiniFlex 600. FTIR spectroscopy was used to collect infrared spectrum of transmittance to identify the different functional groups present in the raw coconut shell particle and carbonized particle. The technique was employed using Nicolet 6700 FT-IR Spectrometer.

#### 2.6 SEM observation

The surface morphology of the precursor (raw coconut) and char (CCSP) was characterized using A high-resolution Quanta 3D FEG FIB/SEM Dual Beam system. The raw coconut particle was coated with a thin layer of gold to make it conductive.

To examine the extent of damage of laminated composites, the fractured surface of composites after tensile test was sectioned for SEM analysis. A thin layer of gold (-5nm) was sputtered on the fractured surface and an acceleration voltage of 15kV was used for imaging.

## 3. Results and Discussions

# 3.1 Powder characterization results

Figure 1 shows images obtained from Scanning Electron Microscopy of raw coconut shell powder (a, b) and carbonized particle (c, d) at different magnifications. The surface morphology of both samples has distinct characteristics. The SEM image of precursor, referred to as raw coconut shell particle in Figure 1(a, b) show the fibrous nature of coconut shell with no pores. Carbonized coconut shell particle in Figure 1(c, d) show rudimentary pores resulting from the burning off of volatiles, namely, moisture, hemicellulose, cellulose and lignin in the raw coconuts during heating [35]. The presence of voids can provide free access of epoxy and promote uniform dispersion. The special structure of coconut biomass shortens the mass transport path and minimizes the diffusion resistance of target substances, which can result in significant improvement in mechanical properties. The darkening nature of the carbonized particle results from the carbonization process.

Figure 2a shows XRD pattern obtained for raw coconut particles before carbonization. The predominant peaks are observed between  $10^{\circ}$  - $20^{\circ}$ ,  $20^{\circ}$  - $25^{\circ}$  and  $30^{\circ}$  - $40^{\circ}$  which represents SiO<sub>2</sub>, C, and CaO respectively [36], with carbon having the highest intensity of about 7,000 cps. The higher carbon content in coconut shell compared to other agriculture biomass makes it attractive for use as biofiller [37]. There are also traces of K<sub>2</sub>O and Fe<sub>2</sub>O<sub>3</sub> peaks occurring at  $2\theta$  of  $27^{\circ}$  and

44° respectively[36]. After carbonization, the XRD analysis of carbonized particle is represented as shown in *Figure 2*b. The diffraction of sample showed two peaks observed at  $2\theta = 23^{\circ}$  and  $43^{\circ}$ ; a characteristic of coconut shell charcoal [35,36].

The diffraction pattern was further analyzed by comparing to literature and it was observed that the resulting char has the same peak position as reduced graphene oxide [37-39]. The diffraction peak at  $2\theta = 23^{\circ}$  in *Figure 2*b is related to the (2 0 0) plane of reduced graphene oxide and its broad nature can be attributed to a randomly arranged crystal phase. A less intense peak found at 43° in the carbonized particle with (0 0 1) crystal phase is a result of a turbostratic band that corresponds to diffraction patterns of amorphous graphitic carbon material [43], [44].

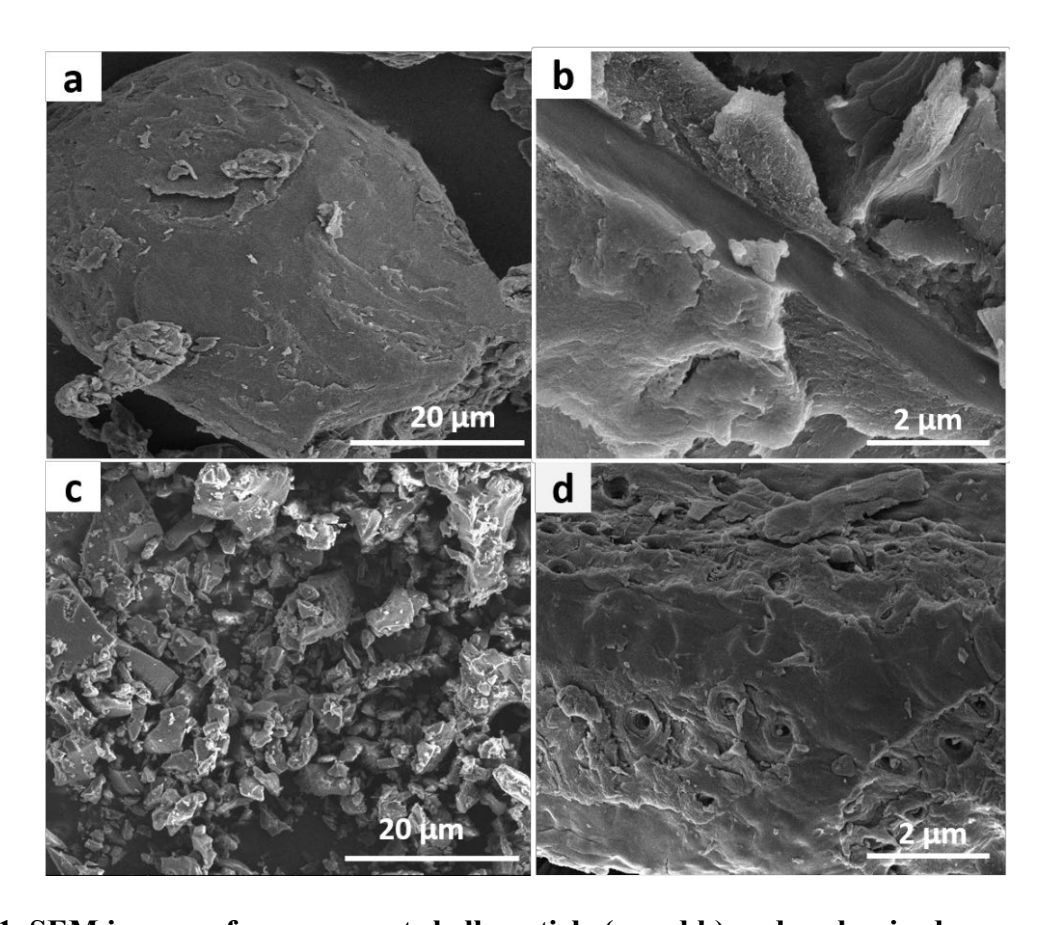


Figure 1. SEM images of raw coconut shell particle (a and b) and carbonized coconut shell particle (c and d)

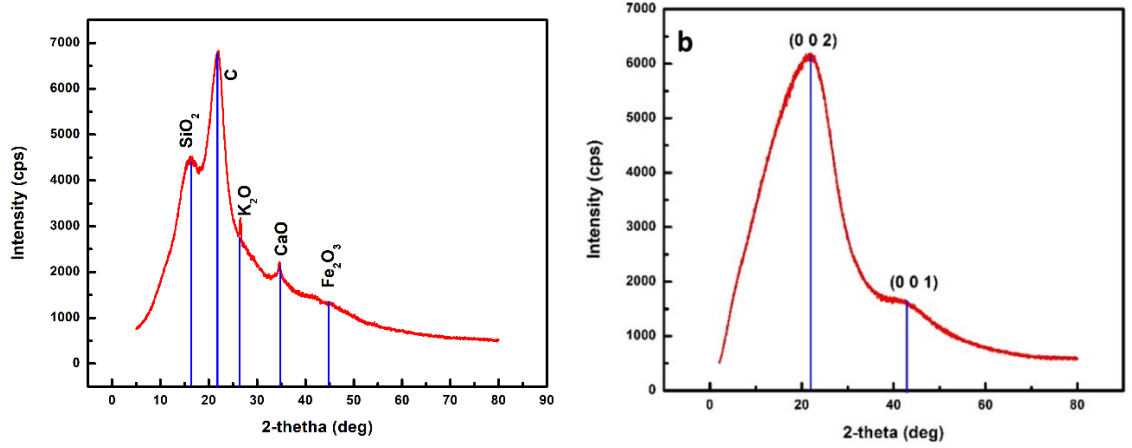


Figure 2. XRD spectra of (a) raw coconut shell particle (b) carbonized coconut shell particle

The Fourier Transform Infrared Spectroscopy (FTIR) of the precursor coconut (raw coconut) and CCSP is shown in *Figure 3*. The IR spectrum of the raw coconut shows the largest peak of -OH stretching at a wavelength of around 3350 cm<sup>-1</sup> as a result of extensive hydrogen bonding in cellulose and hemicellulose [45]. The band at 2920 cm<sup>-1</sup> is a characteristic peak of C-H (alkanes and alkenes) in cellulose and hemicellulose [46]. The band stretching around 1728 cm<sup>-</sup> <sup>1</sup> can be attributed to C=O group of carboxyl aldehyde in lignin and acetyl ester group in cellulose and hemicellulose [42,43]. C=C peak is found around absorbance of 1620 cm<sup>-1</sup> [45]. The band peak stretching between 1500 and 1535 may represent aromatic ring vibrations in lignin, and that at 1450 cm<sup>-1</sup> represents O-CH<sub>3</sub> stretching also found in lignin [45]. The peak found at 1256 cm<sup>-1</sup> may be ascribed to C-O of acetyl group in lignin and hemicellulose. The sharp peak at absorbance of 1020 cm<sup>-1</sup> is associated with C-O and O-H vibrations with respect to polysaccharides in cellulose [47]. The FTIR spectra of CCSP show band stretching of C=C and C-O at 1600 and 1247 cm<sup>-1</sup>, respectively, and residual of C=O, which is a characteristic of molecular bonding in reduced graphene oxide [38,44]. It is observed that the band stretching related to cellulose, hemicellulose, and lignin occurring at 3350 cm<sup>-1</sup>, 2920 cm<sup>-1</sup>, and 1728 cm<sup>-1</sup> in the raw coconut shell powder is either absent or significantly reduced after carbonization in CCSP. These hydroxyl groups are hydrophilic and affects compatibility and water absorption properties.

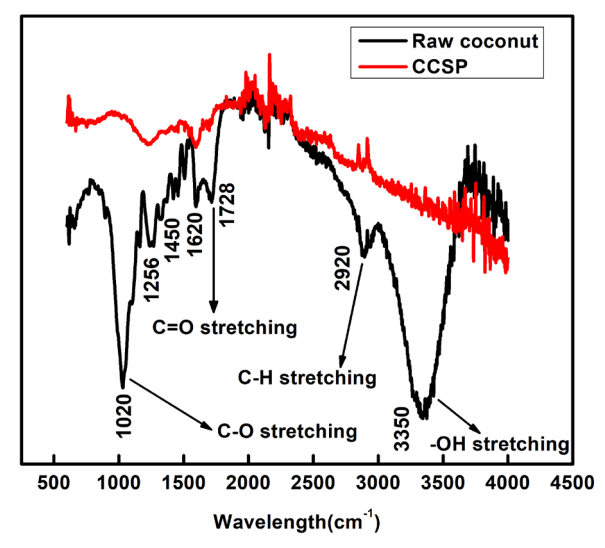


Figure 3. FTIR Image of raw coconut particle and carbonized particle

## 3.2 Tensile test results

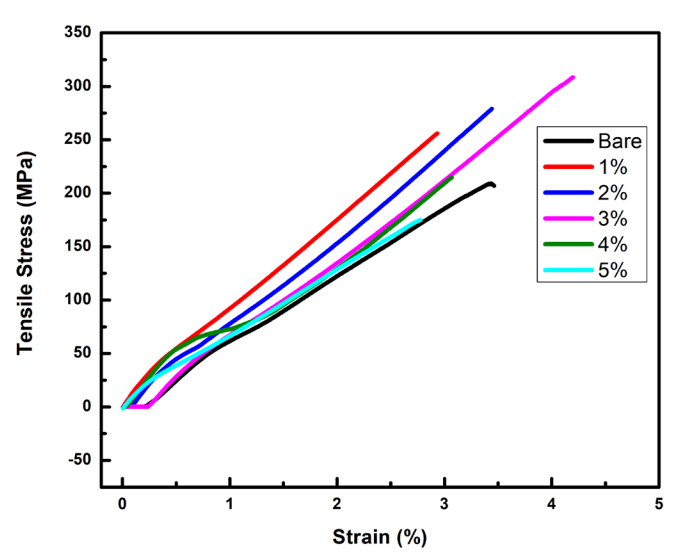


Figure 4. Typical tensile stress-strain curve of reference (Bare) CFRP and hybrid biocomposites

Tensile testing was performed using an MTS at a strain rate of 2mm/min. *Figure 4* shows a typical stress-strain curve for reference CFRP and hybrid biocomposites.

All composite systems, both reference (Bare) and hybrid biocomposites exhibit an elastic tensile behavior; they do not exhibit strain-hardening, and the ultimate strength is the same as strength at failure which is very typical of brittle materials. However, the fracture toughness is enhanced at lower concentrations of carbonized particles evident from the increase in strain at failure. It is observed that, at CCSP concentration of 2% and 3%, the strain at failure is increased in comparison to the reference CFRP. The percentage strain to failure of the composites is shown in *Table 1*. The strain to failure is increased by 23% and 36% with 2% and 3% CCSP, respectively. The enhanced strain to failure with the addition of CCSP is due to enhanced matrix-fiber interfacial

bond. The stiffness of carbon fiber is significantly higher than epoxy in the reference composite based on bare epoxy. This disparity at the matrix/fiber interface increases stress concentration and acts as crack initiation sites leading to early failure. However, with the modified CCSP epoxy matrix, the difference in stiffness between the matrix and fiber is reduced, leading to reduce interfacial stress concentration, and thereby, mitigating the propagation of crack along the fiber/matrix interface [49]. Hence, an increase in strain at failure. Table 1 also shows the tensile strength and stiffness of the reference CFRP and hybrid biocomposites with different CCSP loadings. Tensile strength increased with the addition of carbonized particle with an optimum strength of 288MPa at 3% CCSP loading—an increase of about 36% more than the reference composite. The increase in strength is attributed to reduced interfacial stress concentration between the matrix and the fiber effected by CCSP. This allows for effective transfer of load from the matrix to the fiber; the main load-carrying component of the composite. At higher loadings above 3%, the tensile strength decreases, which can be attributed to agglomeration of particles; increasing the concentration of particles in the matrix resin increases the viscosity of matrix which affects the cure rate and molecular network formation [3], [12]. Agglomerates instigate early failure at the matrix-particle interface by acting as stress concentration centers under loading, which cause significant interfacial stress concentration. The elastic modulus is also increased by 24% and 30% with the addition of 1% and 2% CCSP. There is a slight decrease from 2% CCSP as the concentration increases, however, the stiffness of all the hybrid composites is higher than that of the reference composite.

Table 1 Tensile and flexural test results of reference CFRP and hybrid biocomposites

	Tensile Strain to Failure (%)	Tensile Strength (MPa)	Tensile Modulus (MPa)	Flexural Strength (MPa)	Flexural Modulus (GPa)
Bare	3.5±0.05	211±12	6080±158	87±7	$6.54\pm0.3$
1%	$3.0\pm0.08$	240±11	7532±176	227±15	11.80±0.6
2%	3.7±0.16	268±14	7897±209	245±9	13.14±0.3
3%	4.1±0.12	288±15	7163±247	233±5	$13.68\pm0.6$
4%	3.1±0.07	202±10	6231±142	226±7	13.86±0.2
5%	2.4±0.23	164±17	6090±83	189±3	14.21±0.5

## 3.3 SEM observation of fracture surfaces after tensile tests

The fracture surface of the laminates based on bare epoxy and 2% carbonized particle composite was comparatively analyzed using SEM as shown in *Figure 5* and *Figure 6* respectively. Fiber breakage, fiber pullout, delamination, and fiber-matrix interfacial debonding are observed in both the reference composite and hybrid biocomposite. However, there is a significant difference in the matrix deformation and fiber-matrix adhesion in both composites. The river pattern deformation, and smooth fracture surface observed in *Figure 5* (a, b) are indication of brittle fracture in reference CFRP with bare epoxy matrix. On the other hand, the rough and ductile deformation of matrix as seen in *Figure 6*(a, b) are signs of better fracture toughness compared to the reference composite. The ductile fracture of fiber-matrix interface in *Figure 6*b shows a good fiber-matrix adhesion in hybrid composite, thus there is a strong bond between the fiber and matrix. The smooth fracture and complete fiber-matrix debonding in *Figure 5* of the reference composite shows the poor bonding at its fiber-matrix interface.

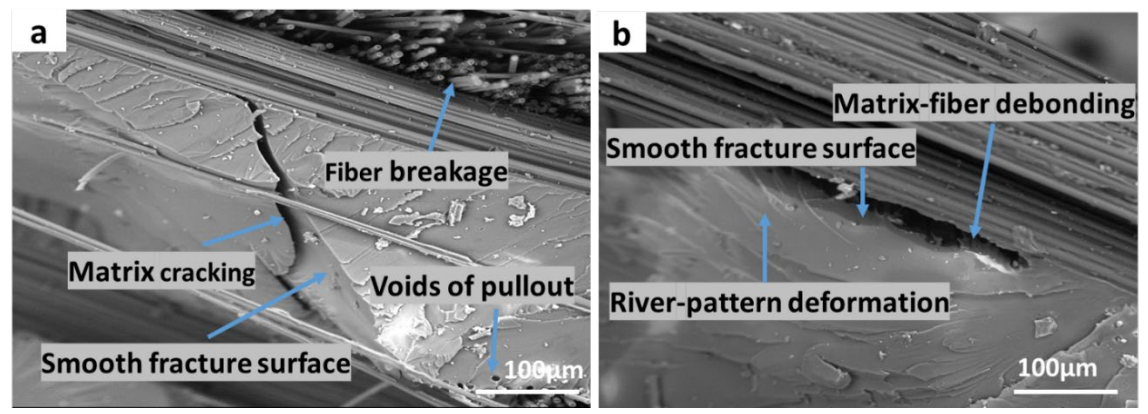


Figure 5. SEM image of fracture surface of reference CFRP after tensile testing. a and b are images taken at different positions

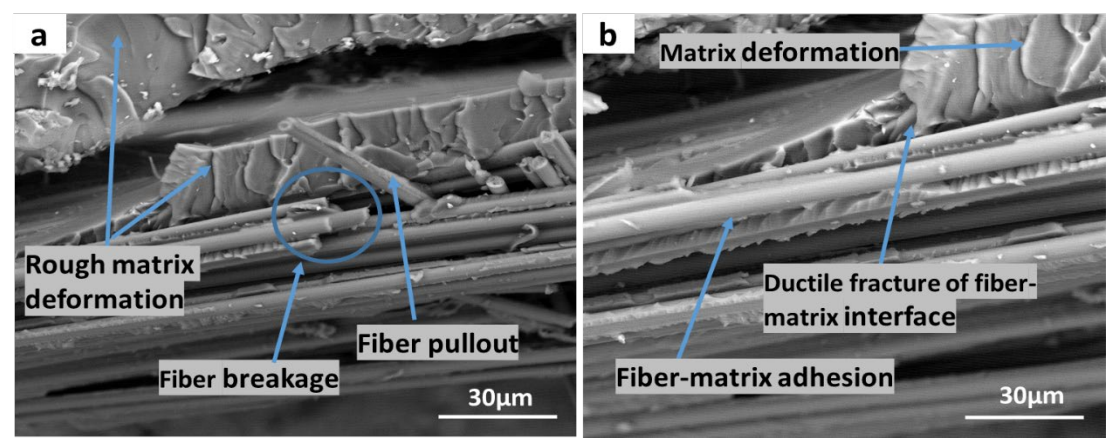


Figure 6. SEM images of fractures surface of hybrid biocomposite after tensile testing. a and b are images taken at different positions

#### 3.4 Flexural test results

Table 1 also summarizes the flexural strength and flexural modulus of hybrid biocomposites at different CCSP loadings compared to the reference CFRP based on bare epoxy. It can be observed that, all hybrid biocomposites have higher flexural strength than the reference CFRP. The flexural strength of the biocomposites increases with increasing CCSP loading up to 2%, where the optimum flexural strength of 245MPa is obtained and decreases slightly as the concentration of the CCSP increases.

As discussed early in the tensile test result, good dispersion at lower CCSP loadings increases the interfacial bonding between the matrix and fiber. Addition of particles to the matrix causes roughness on the surface of the fiber without causing damage to the fiber surface. Surface roughness together with good interfacial adhesion provides mechanical interlocking and enhanced frictional coefficient which leads to increased flexural strength [1]. The particles also help in the deflection of cracks which increases the resistance to delamination. The decrease in strength at higher loadings may be due to agglomeration. Another factor contributing to the decrease in strength may be due to the large surface area available for the entrapment of air bubbles from the atmosphere, and restriction to the escape of volatile gases [10], [50], which compromises with the net strength of the composite. The flexural modulus as shown in *Table 1* is also increased in the

hybrid biocomposites with increasing CCSP loadings. Addition of carbonized particles to the epoxy resin increases the stiffness of the matrix which translates into higher stiffness of the hybrid bio-composite according to the rule of mixtures.

# 3.5 Low Velocity Impact Test Result

The impact behavior of the composites was analyzed using time to completion of impact event, deflection, peak load, initiation energy and crack propagation energy. *Figure 7* shows the load-deflection response of the impact event associated with the various forms of composites. It can be observed that, there is a linear increase in force until a Hertzian failure is experienced. The Hertzian failure is usually attributed to matrix cracking in the area of contact [51]. The reference CFRP starts to fail at around 780N, consequence of the brittle nature of the epoxy. However, with addition of biofillers to the matrix of the hybrid biocomposites, the matrix is toughened, and crack propagation is mitigated which is evident in the higher loads of biocomposites before failure is initiated.

The slope of the contact force against displacement is called bending stiffness and it describes resistance to impact loading [13,46-48]. Higher slope values are observed for composites based on CCSP, indication of higher stiffness resulting from increased stiffness of the matrix. After the maximum force is reached, there is a sudden drop and fluctuations of the contact force. Past research has attributed this sudden drop and fluctuations to the initiation of failure in the form of delamination, fiber breakage and/or fiber pullout.

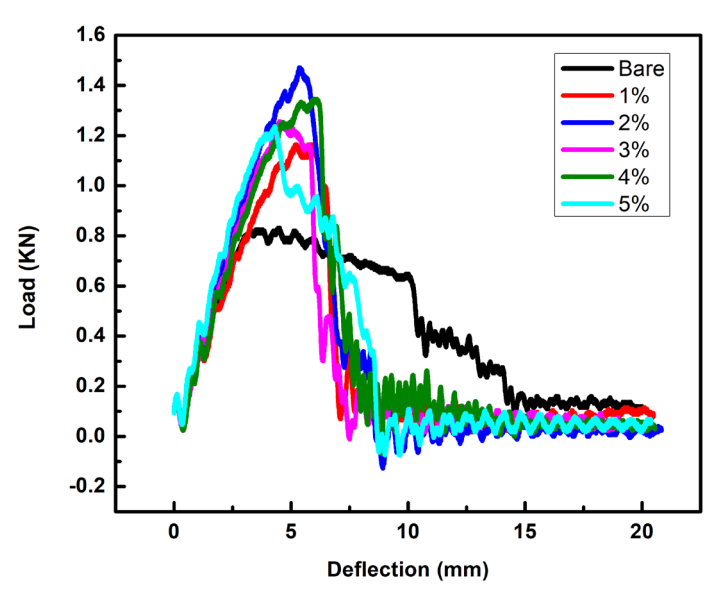


Figure 7. Load versus deflection curve of the reference CFRP and hybrid biocomposites with different CCSP loadings

The impact duration, maximum deflection, peak impact force, initiation energy, and propagation energy are summarized in *Table 2*.

The maximum impact force, referred to as peak force in the load-deflection curve, represents the amount of a load a composite laminate can withstand before undergoing crucial damage. From the Table, the hybrid biocomposites have higher peak force when compared to the reference CFRP. The peak load of the reference CFRP has been increased between 46% - 80%

with the addition of CCSP as shown in *Table 2*. The lower peak force in the reference composite can be associated with early delamination and debonding.

The time to completion of the impact event is also an indication of the stiffness of the material; compliant materials take longer time to complete an impact event, while the time to completion for stiffer materials occur earlier [54]. From *Table 2*, the reference CFRP takes a much longer time to complete the impact event relative to the hybrid biocomposites with 1wt, 2wt%, and 3wt% CCSP. This is also echoed by the maximum deflection. The reference CFRP has much larger deflection than the biocomposites, suggesting that the biocomposites have much higher bending stiffness, which is also proved by the bending test results as given in *Table 1*.

In any impact event, when the striker hits the sample, the initial stage of energy absorption is through elastic deformation. As the maximum elastic deformation is reached, the excess energy is absorbed in the form of plastic deformation in ductile materials or damage formation with brittle materials [54]. In essence, the maximum impact energy is a total of energy absorbed elastically, energy absorbed in the formation of damages and as consequence of friction between sample and striker. To better understand the impact tolerance, the initiation energy and propagation energy are used.

Table 2 Average value of results obtained from low velocity impact test

	Time (ms)	Displacement		Initiation	Propagation
		(mm)	force (N)	energy (J)	energy (J)
Bare	$14.29 \pm 0.88$	$7.45 \pm 0.55$	792±96	$2.42\pm0.45$	$8.84 \pm 0.96$
1%	$7.71 \pm 0.85$	$3.92 \pm 0.81$	1163±77	$3.50\pm0.35$	$3.72\pm0.64$
2%	$7.62 \pm 0.57$	$4.01\pm0.31$	1432±39	$4.43 \pm 0.08$	$3.20\pm0.55$
3%	$7.56\pm1.02$	$3.90\pm1.07$	1384±33	$3.69\pm0.77$	$5.09\pm0.69$
4%	8.23±0.94	$4.12\pm0.87$	1371±52	$3.58\pm0.26$	$4.06\pm1.04$
5%	8.75±1.07	4.30±1.02	1267±31	3.17±0.06	$5.12\pm0.82$

Figure 8 shows a typical impact load and impact energy against time graph showing maximum impact energy and initiation energy. The initiation energy is the energy at the maximum load while the propagation energy is the difference between the maximum impact energy and initiation energy [55]. Initiation energy describes the ability for the target to transfer energy elastically while propagation energy is the amount of energy absorbed by the target in the generation and propagation of damages [51,52]. Briefly, a higher initiation energy and/or lower propagation energy suggests a good and higher impact tolerance. On the other hand, a higher propagation energy and/or lower initiation indicates an enormous impact damage.

Table 2 reports the initiation energy and propagation energy of the hybrid biocomposites compared to the reference CFRP. The reference CFRP based on bare epoxy matrix has the highest propagation energy of 8.84J indicating a larger impact damage. The hybrid biocomposite with 2wt% CCSP has the highest initiation energy which suggests that the laminate transfers elastic energy better than the other laminates. This is because of good dispersion of CCSP particles and enhanced fracture toughness as discussed in the tensile test results. 2wt% CCSP hybrid composite also has the least propagation energy of 3.20J which implies a lesser impact damage compared to other composites. The hybrid biocomposite with 2wt% CCSP gives the optimum impact tolerance.

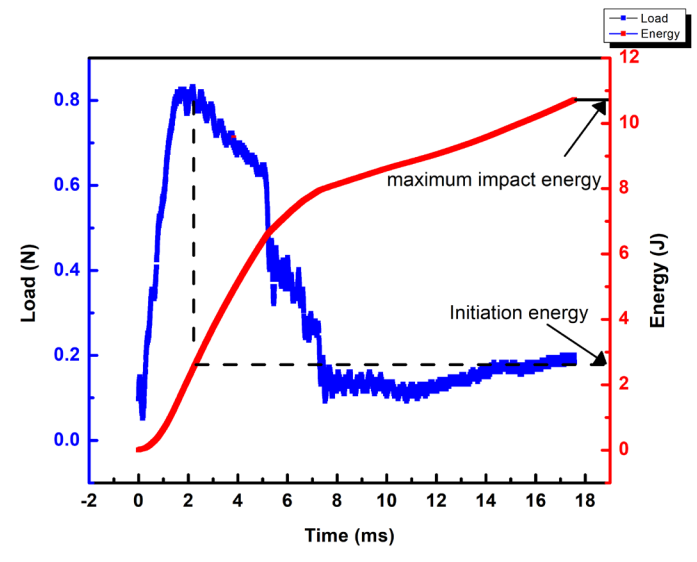
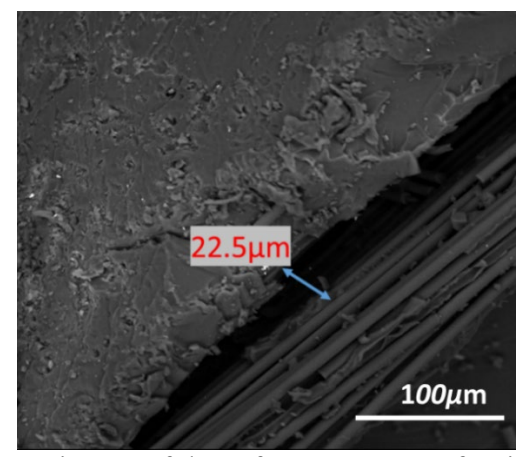
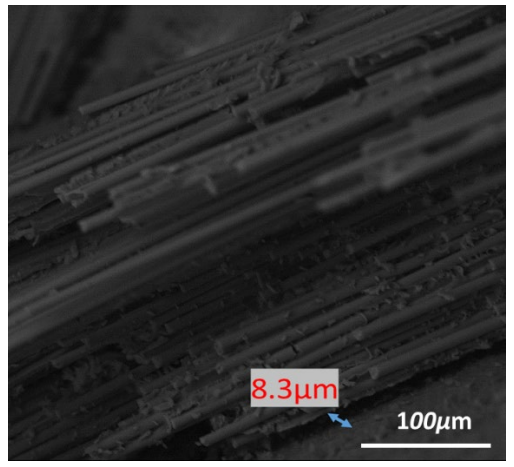


Figure 8. Typical impact load and impact energy against time curve of a composite

To corroborate the extent of failure of the hybrid biocomposites compared to the reference CFRP, the surface of laminates was examined under SEM after impact. *Figure 9*(a, b) show the SEM images of the reference CFRP and 2wt% CCSP hybrid biocomposite, respectively. *Figure 9*a illustrates that, the reference CFRP based on bare epoxy matrix has undergone severe damage which is evident from the larger openings of delamination. This is commensurate with the maximum deflection and propagation energy results obtained, because of the poor out-of-plane behavior of the CFRP. On the other hand, from *Figure 9*b, delamination opening in the hybrid composite is narrower, hence lesser damage experienced. This results from the good fiber-matrix adhesion effected by the addition of CCSP to the matrix of the hybrid composites, thereby enhancing its out-of-plane performance. This is observed in the higher initiation energy, lesser propagation energy and lower deflection results obtained for the hybrid biocomposites, 2wt% CCSP loading.



(a) SEM image of the reference CFRP after impact



(b) SEM image of the hybrid biocomposite after impact

Figure 9. SEM observation of the composites after the low velocity impact (a) the reference CFRP and (b) the biocomposite

#### 4. Conclusion

Carbonized particles from coconut shell have been incorporated into the epoxy matrix of CFRP to fabricate five hybrid biocomposites with different weight compositions of carbonized particles: 1%, 2%, 3%, 4%, and 5%. The mechanical performance of the hybrid biocomposites were compared to a reference CFRP which was based on bare epoxy and carbon fiber without carbonized particles. The following conclusions were drawn after tensile, flexural, and low velocity impact tests.

- The tensile fracture toughness, tensile strength and elastic modulus were enhanced with the addition of carbonized particles at lower CCSP loadings compared to the reference CFRP. However, at higher CCSP loadings, the properties are compromised because of particle agglomeration.
- SEM analysis of the fractured surface showed better fiber-matrix adhesion in the hybrid biocomposites relative to the reference CFRP.
- The flexural strength and stiffness were enhanced in hybrid biocomposites in comparison to the reference CFRP.
- The reference CFRP experienced severe damage during impact test with higher propagation energy, larger deflection, and lower initiation energy. Addition of 2wt% CCSP to the epoxy matrix gives optimum impact tolerance with higher initiation energy, lowest propagation energy, and minimum deflection.

## Acknowledgement

This work was supported by the National Science Foundation CREST program through cooperative agreement HRD 1736136, National Science Foundation under grant number OIA-1946231 and the Louisiana Board of Regents for the Louisiana Materials Design Alliance (LAMDA).

#### References

- [1] M. Hussain, A. Nakahira, and K. Niihara, "Mechanical property improvement of carbon fiber reinforced epoxy composites by Al2O3 filler dispersion," *Mater. Lett.*, vol. 26, no. 3, pp. 185–191, 1996, doi: 10.1016/0167-577X(95)00224-3.
- [2] K. J. Green, D. R. Dean, U. K. Vaidya, and E. Nyairo, "Multiscale fiber reinforced composites based on a carbon nanofiber/epoxy nanophased polymer matrix: Synthesis, mechanical, and thermomechanical behavior," *Compos. Part A Appl. Sci. Manuf.*, vol. 40, no. 9, pp. 1470–1475, 2009, doi: 10.1016/j.compositesa.2009.05.010.
- [3] B. Ashrafi *et al.*, "Enhancement of mechanical performance of epoxy/carbon fiber laminate composites using single-walled carbon nanotubes," *Compos. Sci. Technol.*, vol. 71, no. 13, pp. 1569–1578, 2011, doi: 10.1016/j.compscitech.2011.06.015.
- [4] H. Ulus, T. Üstün, Ö. S. Sahin, S. E. Karabulut, V. Eskizeybek, and A. Avcl, "Low-velocity impact behavior of carbon fiber/epoxy multiscale hybrid nanocomposites reinforced with multiwalled carbon nanotubes and boron nitride nanoplates," *J. Compos. Mater.*, vol. 50, no. 6, pp. 761–770, 2016, doi: 10.1177/0021998315580835.
- [5] D. Cao, S. Malakooti, V. N. Kulkarni, Y. Ren, and H. Lu, "Nanoindentation measurement of core–skin interphase viscoelastic properties in a sandwich glass composite," *Mech. Time-Dependent Mater.*, vol. 25, no. 3, pp. 353–363, 2021, doi: 10.1007/s11043-020-09448-y.
- [6] D. Cao *et al.*, "The effect of resin uptake on the flexural properties of compression molded sandwich composites," *Wind Energy*, vol. 25, no. 1, pp. 71–93, 2022, doi: 10.1002/we.2661.
- [7] H. Q. Afful, S. Ibekwe, P. Mensah, and G. Li, "Influence of uniaxial compression on the shape memory behavior of vitrimer composite embedded with tension-programmed unidirectional shape memory polymer fibers," *J. Appl. Polym. Sci.*, vol. 138, no. 20, pp. 1–9, 2021, doi: 10.1002/app.50429.
- [8] L. Penn and H. Wang, *Handbook of Composites*, 2 edition. Great Britian: Chapman & Hall, 1998.
- [9] D. Carolan, A. Ivankovic, A. J. Kinloch, S. Sprenger, and A. C. Taylor, "Toughened carbon fibre-reinforced polymer composites with nanoparticle-modified epoxy matrices," *J. Mater. Sci.*, vol. 52, no. 3, pp. 1767–1788, 2017, doi: 10.1007/s10853-016-0468-5.
- [10] A. Mohanty, V. K. Srivastava, and P. U. Sastry, "Investigation of mechanical properties of alumina nanoparticle-loaded hybrid glass/carbon-fiber-reinforced epoxy composites," *J. Appl. Polym. Sci.*, vol. 131, no. 1, pp. 1–7, 2014, doi: 10.1002/app.39749.
- [11] A. Mohanty and V. K. Srivastava, "Effect of alumina nanoparticles on the enhancement of impact and flexural properties of the short glass/carbon fiber reinforced epoxy based composites," *Fibers Polym.*, vol. 16, no. 1, pp. 188–195, 2015, doi: 10.1007/s12221-015-0188-5.
- [12] V. Sivabharathi, G. S. Chidambaram, N. Sadayan, and S. Ashokraj, "Enhanced mechanical properties of glass fibre-reinforced polymer composites with addition of AL2O3," *Aust. J. Mech. Eng.*, vol. 00, no. 00, pp. 1–9, 2019, doi: 10.1080/14484846.2019.1681848.
- [13] R. K. Nayak, A. Dash, and B. C. Ray, "Effect of Epoxy Modifiers (Al 2 O 3 /SiO 2 /TiO 2 ) on Mechanical Performance of epoxy/glass Fiber Hybrid Composites," *Procedia Mater. Sci.*, vol. 6, no. Icmpc, pp. 1359–1364, 2014, doi: 10.1016/j.mspro.2014.07.115.
- [14] S. Nallusamy, "Characterization of epoxy composites with TiO2 additives and E-glass fibers as reinforcement agent," *J. Nano Res.*, vol. 40, pp. 99–104, 2015, doi:

- 10.4028/www.scientific.net/JNanoR.40.99.
- [15] M. T. Demirci, "Low velocity impact and fracture characterization of SiO2 nanoparticles filled basalt fiber reinforced composite tubes," *J. Compos. Mater.*, vol. 54, no. 23, pp. 3415–3433, 2020, doi: 10.1177/0021998320915952.
- [16] Y. Zheng, R. Ning, and Y. Zheng, "Study of SiO2 nanoparticles on the improved performance of epoxy and fiber composites," *J. Reinf. Plast. Compos.*, vol. 24, no. 3, pp. 223–233, 2005, doi: 10.1177/0731684405043552.
- [17] A. Y. Boroujeni, M. Tehrani, A. J. Nelson, and M. Al-Haik, *Hybrid carbon nanotube-carbon fiber composites with improved in-plane mechanical properties*, vol. 66. Elsevier Ltd, 2014.
- [18] A. Godara *et al.*, "Influence of carbon nanotube reinforcement on the processing and the mechanical behaviour of carbon fiber/epoxy composites," *Carbon N. Y.*, vol. 47, no. 12, pp. 2914–2923, 2009, doi: 10.1016/j.carbon.2009.06.039.
- [19] E. J. Garcia, B. L. Wardle, A. John Hart, and N. Yamamoto, "Fabrication and multifunctional properties of a hybrid laminate with aligned carbon nanotubes grown In Situ," *Compos. Sci. Technol.*, vol. 68, no. 9, pp. 2034–2041, 2008, doi: 10.1016/j.compscitech.2008.02.028.
- [20] F. Gojny, M. Wichmann, B. Fiedler, B. W, and K. Schulte, "Influence of nano-modification on the mechanical and electrical properties of conventional fiber-reinforced composites.," *Compos Part A-Appl S*, vol. 36.
- [21] X. Wang *et al.*, "The Interfacial Shear Strength of Carbon Nanotube Sheet Modified Carbon Fiber Composites," *Conf. Proc. Soc. Exp. Mech. Ser.*, vol. 2, pp. 25–32, 2021, doi: 10.1007/978-3-030-59542-5\_4.
- [22] R. Udhayasankar and B. Karthikeyan, "A review on coconut shell reinforced composites," *Int. J. ChemTech Res.*, vol. 8, no. 11, pp. 624–637, 2015.
- [23] T. Berhanu and S. Gebresilasiea, "Physical and Mechanical Behavior of Sisal Fiber Reinforced Polyester Matrix Composites," vol. 1, no. 2, pp. 128–142, 2020.
- [24] G. U. Raju and S. Kumarappa, "Experimental study on mechanical properties of groundnut shell particle-reinforced epoxy composites," *J. Reinf. Plast. Compos.*, vol. 30, no. 12, pp. 1029–1037, 2011, doi: 10.1177/0731684411410761.
- [25] A. Yadav and M. K. Gupta, "Development and characterization of jute composites for sustainable product: Effect of chemical treatments and polymer coating," *Mater. Res. Express*, vol. 7, no. 1, 2019, doi: 10.1088/2053-1591/ab5bd9.
- [26] S. L. Fávaro, M. S. Lopes, A. G. Vieira de Carvalho Neto, R. Rogério de Santana, and E. Radovanovic, "Chemical, morphological, and mechanical analysis of rice husk/post-consumer polyethylene composites," *Compos. Part A Appl. Sci. Manuf.*, vol. 41, no. 1, pp. 154–160, 2010, doi: 10.1016/j.compositesa.2009.09.021.
- [27] K. Rassiah and M. M. H. M. Ahmad, "A Review On Mechanical Properties Of Bamboo Fiber Reinforced Polymer Composite," vol. 7, no. 8, pp. 247–253, 2013.
- [28] R. F. Gibson, "A review of recent research on mechanics of multifunctional composite materials and structures," *Compos. Struct.*, vol. 92, no. 12, pp. 2793–2810, 2010, doi: 10.1016/j.compstruct.2010.05.003.
- [29] J. O. Akindapo, A. Harrison, and O. M. Sanusi, "Evaluation of Mechanical Properties of Coconut Shell Fibres as Reinforcement Material in Epoxy Matrix," *Int. J. Eng. Res. Technol.*, vol. 3, no. 2, pp. 2337–2348, 2014, [Online]. Available: www.ijert.org.
- [30] T. M. Somashekhar, P. Naik, V. Nayak, Mallikappa, and S. Rahul, "Study of Mechanical Properties of Coconut Shell Powder and Tamarind Shell Powder Reinforced with Epoxy

- Composites," *IOP Conf. Ser. Mater. Sci. Eng.*, vol. 376, no. 1, 2018, doi: 10.1088/1757-899X/376/1/012105.
- [31] J. O. Agunsoye, A. K. Odumosu, and O. Dada, "Novel epoxy-carbonized coconut shell nanoparticles composites for car bumper application," *Int. J. Adv. Manuf. Technol.*, vol. 102, no. 1–4, pp. 893–899, 2019, doi: 10.1007/s00170-018-3206-0.
- [32] U. C. Mark, I. C. Madufor, H. C. Obasi, and U. Mark, "Influence of filler loading on the mechanical and morphological properties of carbonized coconut shell particles reinforced polypropylene composites," *J. Compos. Mater.*, vol. 54, no. 3, pp. 397–407, 2020, doi: 10.1177/0021998319856070.
- [33] ASTM, "D3039/D3039M-17: Standard Test Method for Tensile Properties of Polymer Matrix Composite Materials," *Annu. B. ASTM Stand.*, pp. 1–13, 2017, [Online]. Available: http://scholar.google.com/scholar?hl=en&btnG=Search&q=intitle:Standard+Test+Method +for+Tensile+Properties+of+Polymer+Matrix+Composite+Materials#1.
- [34] J. M. F. de Paiva, S. Mayer, and M. C. Rezende, "Comparison of tensile strength of different carbon fabric reinforced epoxy composites," *Mater. Res.*, vol. 9, no. 1, pp. 83–89, 2006, doi: 10.1590/s1516-14392006000100016.
- [35] N. S. Nasri, M. Jibril, M. A. A. Zaini, R. Mohsin, H. U. Dadum, and A. M. Musa, "Synthesis and characterization of bio-based porous carbons by two step physical activation with CO2," *J. Teknol. (Sciences Eng.*, vol. 68, no. 5, pp. 5–9, 2014, doi: 10.11113/jt.v68.3022.
- [36] I. Ismail, Arliyani, S. Fathmiyah, Mursal, Z. Jalil, and H. P. S. A. Khalil, "Effect of ball-milling time on chemical property of coconut shell powder," *J. Phys. Conf. Ser.*, vol. 1572, no. 1, 2020, doi: 10.1088/1742-6596/1572/1/012021.
- [37] M. Jahan and F. Feni, "Environmentally Friendly Bifunctional Catalyst for ORR and OER from Coconut Shell Particles," *Adv. Mater. Phys. Chem.*, vol. 12, no. 05, pp. 106–123, 2022, doi: 10.4236/ampc.2022.125008.
- [38] K. W. Mas'Udah, I. M. A. Nugraha, S. Abidin, A. Mufid, F. Astuti, and Darminto, "Solution of reduced graphene oxide synthesized from coconut shells and its optical properties," *AIP Conf. Proc.*, vol. 1725, no. May, 2016, doi: 10.1063/1.4945499.
- [39] D. N. Jayanti, A. Y. Nugraheni, Kurniasari, M. A. Baqiya, and Darminto, "Photoluminescence of Reduced Graphene Oxide Prepared from Old Coconut Shell with Carbonization Process at Varying Temperatures," *IOP Conf. Ser. Mater. Sci. Eng.*, vol. 196, no. 1, 2017, doi: 10.1088/1757-899X/196/1/012005.
- [40] C. Fu, G. Zhao, H. Zhang, and S. Li, "Evaluation and characterization of reduced graphene oxide nanosheets as anode materials for lithium-ion batteries," *Int. J. Electrochem. Sci.*, vol. 8, no. 5, pp. 6269–6280, 2013.
- [41] M. Strankowski, D. Włodarczyk, Ł. Piszczyk, and J. Strankowska, "Polyurethane Nanocomposites Containing Reduced Graphene Oxide, FTIR, Raman, and XRD Studies," *J. Spectrosc.*, vol. 2016, 2016, doi: 10.1155/2016/7520741.
- [42] L. Stobinski *et al.*, "Graphene oxide and reduced graphene oxide studied by the XRD, TEM and electron spectroscopy methods," *J. Electron Spectros. Relat. Phenomena*, vol. 195, pp. 145–154, 2014, doi: 10.1016/j.elspec.2014.07.003.
- [43] N. M. S. Hidayah *et al.*, "Comparison on graphite, graphene oxide and reduced graphene oxide: Synthesis and characterization," *AIP Conf. Proc.*, vol. 1892, no. October, 2017, doi: 10.1063/1.5005764.
- [44] M. Yang *et al.*, "Highly cost-effective nitrogen-doped porous coconut shell-based CO2 sorbent synthesized by combining ammoxidation with KOH activation," *Environ. Sci.*

- Technol., vol. 49, no. 11, pp. 7063–7070, 2015, doi: 10.1021/acs.est.5b01311.
- [45] C. D. Liyanage and M. Pieris, "A Physico-Chemical Analysis of Coconut Shell Powder," *Procedia Chem.*, vol. 16, pp. 222–228, 2015, doi: 10.1016/j.proche.2015.12.045.
- [46] H. Essabir, M. O. Bensalah, D. Rodrigue, R. Bouhfid, and A. Qaiss, "Structural, mechanical and thermal properties of bio-based hybrid composites from waste coir residues: Fibers and shell particles," *Mech. Mater.*, vol. 93, pp. 134–144, 2016, doi: 10.1016/j.mechmat.2015.10.018.
- [47] H. Essabir *et al.*, "Bio-composites based on polypropylene reinforced with Almond Shells particles: Mechanical and thermal properties," *Mater. Des.*, vol. 51, pp. 225–230, 2013, doi: 10.1016/j.matdes.2013.04.031.
- [48] A. Y. Nugraheni, M. Nashrullah, F. A. Prasetya, F. Astuti, and Darminto, "Study on phase, molecular bonding, and bandgap of reduced graphene oxide prepared by heating coconut shell," *Mater. Sci. Forum*, vol. 827, pp. 285–289, 2015, doi: 10.4028/www.scientific.net/MSF.827.285.
- [49] M. Tehrani, A. Y. Boroujeni, T. B. Hartman, T. P. Haugh, S. W. Case, and M. S. Al-Haik, "Mechanical characterization and impact damage assessment of a woven carbon fiber reinforced carbon nanotube-epoxy composite," *Compos. Sci. Technol.*, vol. 75, pp. 42–48, 2013, doi: 10.1016/j.compscitech.2012.12.005.
- [50] A. Mohanty and V. K. Srivastava, "Effect of alumina nanoparticles on the enhancement of impact and flexural properties of the short glass/carbon fiber reinforced epoxy based composites," *Fibers Polym.*, vol. 16, no. 1, pp. 188–195, 2015, doi: 10.1007/s12221-015-0188-5.
- [51] L. Gemi, M. Kayrıcı, M. Uludağ, D. S. Gemi, and Ö. S. Şahin, "Experimental and statistical analysis of low velocity impact response of filament wound composite pipes," *Compos. Part B Eng.*, vol. 149, pp. 38–48, 2018, doi: 10.1016/j.compositesb.2018.05.006.
- [52] I. Taraghi, A. Fereidoon, and F. Taheri-Behrooz, "Low-velocity impact response of woven Kevlar/epoxy laminated composites reinforced with multi-walled carbon nanotubes at ambient and low temperatures," *Mater. Des.*, vol. 53, pp. 152–158, 2014, doi: 10.1016/j.matdes.2013.06.051.
- [53] L. Gemi, M. Kara, and A. Avci, "Low velocity impact response of prestressed functionally graded hybrid pipes," *Compos. Part B Eng.*, vol. 106, pp. 154–163, 2016, doi: 10.1016/j.compositesb.2016.09.025.
- [54] M. V. Hosur, A. A. Mohammed, S. Zainuddin, and S. Jeelani, "Processing of nanoclay filled sandwich composites and their response to low-velocity impact loading," *Compos. Struct.*, vol. 82, no. 1, pp. 101–116, 2008, doi: 10.1016/j.compstruct.2006.12.009.
- [55] G. Li and V. D. Muthyala, "Impact characterization of sandwich structures with an integrated orthogrid stiffened syntactic foam core," *Compos. Sci. Technol.*, vol. 68, no. 9, pp. 2078–2084, 2008, doi: 10.1016/j.compscitech.2008.03.014.
- [56] J. Konlan, P. Mensah, S. Ibekwe, K. Crosby, and G. Li, "Vitrimer based composite laminates with shape memory alloy Z-pins for repeated healing of impact induced delamination," *Compos. Part B Eng.*, vol. 200, p. 108324, 2020, doi: 10.1016/j.compositesb.2020.108324.
- [57] G. Li and V. S. Chakka, "Isogrid stiffened syntactic foam cored sandwich structure under low velocity impact," *Compos. Part A Appl. Sci. Manuf.*, vol. 41, no. 1, pp. 177–184, 2010, doi: 10.1016/j.compositesa.2009.10.007.